

Supporting Information

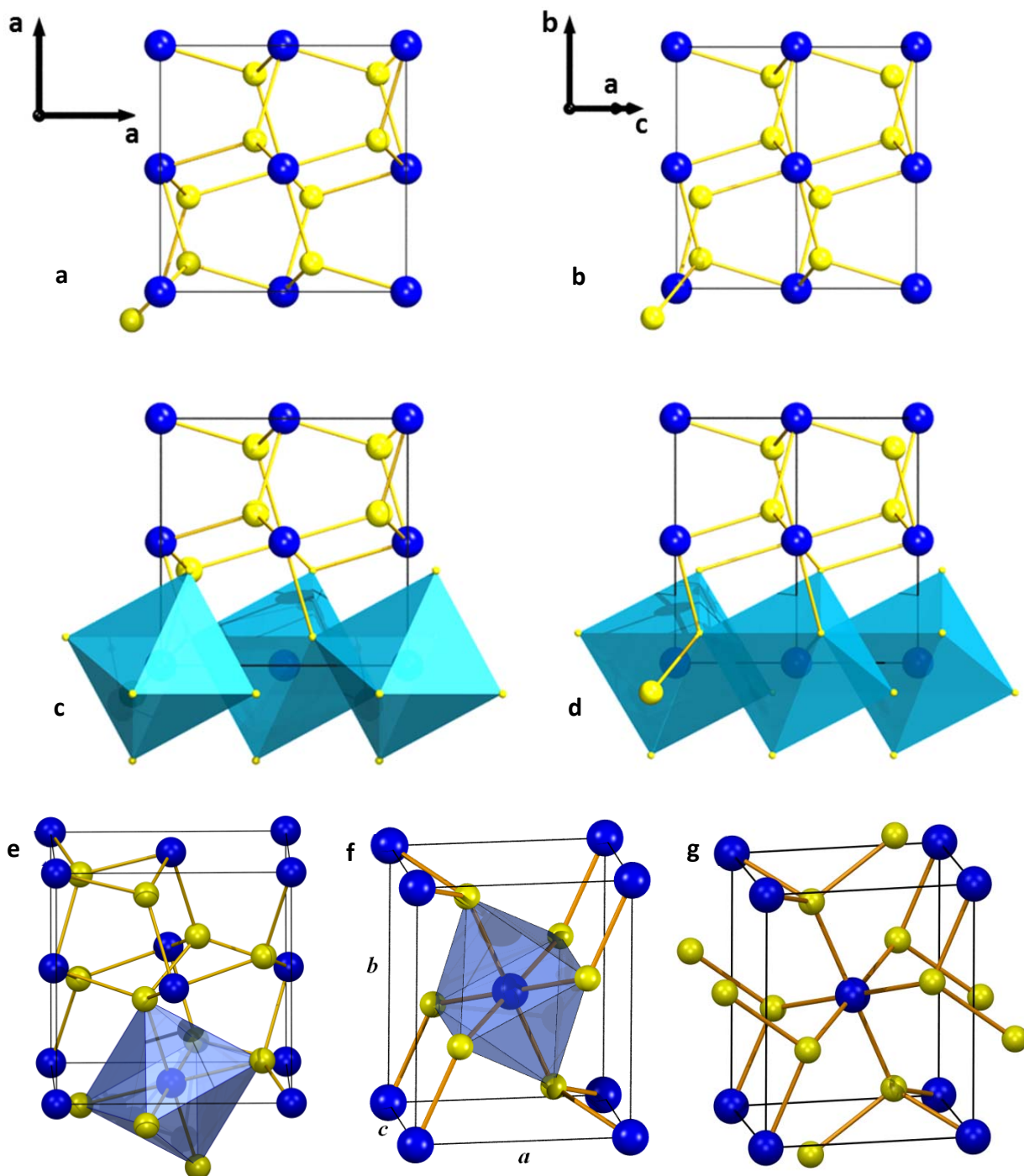


Figure S1: Unit cells of the pyrite (a,c) and the marcasite (b,d) structure illustrating the similarity/differences of the two structures, and depicting one of the FeS₆ octahedra of the structure in each case (e and f). (g) illustrates the S-S interactions in marcasite. Blue spheres represent Fe atoms and yellow spheres represent S atoms.

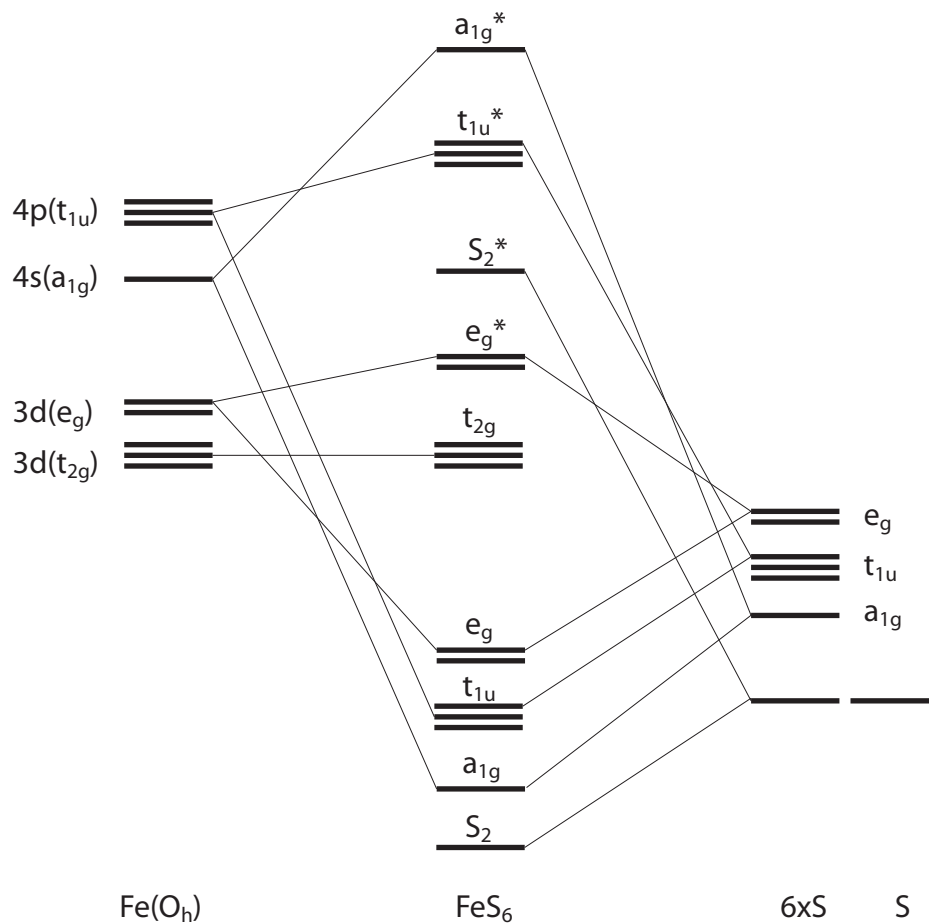


Figure S2: MO-derived qualitative valence band diagram of FeS₂ (neglecting the further splitting of the t_{2g} and e_g levels on Fe) based on the models of Bither *et al.* (1968) and Brostigen and Kjekshus (1970).

I. Multipole refinement against experimental data

Table S1. Atomic positions and ADPs from multipole refinement against experimental pyrite and marcasite data.

		<i>Pyrite</i>	<i>Marcasite</i>
Fe	<i>x, y, z</i>	0	0
	U_{11}	0.00171(1)	0.00147(2)
	U_{22}	0.00171(1)	0.00172(2)
	U_{33}	0.00171(1)	0.00175(2)
	U_{12}, U_{13}, U_{23}	-0.00001(0)	-0.00001(1) (only U12)
S	<i>x</i>	0.384882(6)	0.20003(2)
	<i>y</i>	0.384882(6)	0.37820(1)
	<i>z</i>	0.384882(6)	0
	U_{11}	0.00224(2)	0.00206(3)
	U_{22}	0.00224(2)	0.00225(2)
	U_{33}	0.00224(2)	0.00226(2)
	U_{12}, U_{13}, U_{23}	0.00000(1)	-0.00013(1) (only U12)

Table S2.I. Monopole populations, radial Parameters and net atomic charges for pyrite and marcasite.

		Atom	P_{val}	κ	P_{00}	κ'	Net charge
<i>Pyrite</i>		Fe	6.393(253)	0.976(14)	0	0.990(18)	+1.607(253)
		S	6.803(127)	0.973(10)	0	0.602(30)	-0.803(127)
<i>Marcasite</i>		Fe	5.920(148)	0.995(11)	1.396(226)	1.081(41)	+0.684(374)
		S	6.342(121)	0.977(9)	0.000	0.797(58)	-0.342(121)

Table S2.III. Dipole population parameters for pyrite and marcasite.

		Atom	D_{11+}	D_{11-}	D_{10}	κ'
<i>Pyrite</i>		Fe	0	0	0	0.990
		S	0	0	0.563(287)	0.602
<i>Marcasite</i>		Fe	0	0	0	1.081
		S	0.069(74)	0.041(81)	0	0.797

Table S2.IV. Quadrupole population parameters for pyrite and marcasite.

		Atom	Q_{20}	Q_{21+}	Q_{21-}	Q_{22+}	Q_{22-}
<i>Pyrite</i>		Fe	0.016(9)	0	0	0	0
		S	0.011(1)	0	0	0	0
<i>Marcasite</i>		Fe	-0.011(17)	0	0	-0.044(16)	-0.022(16)
		S	-0.003(65)	0	0	0.125(55)	-0.171(63)

Table S2.V. Octupole population parameters for pyrite and marcasite.

	Atom	O_{30}	O_{31+}	O_{31-}	O_{32+}	O_{32-}	O_{33+}	O_{33-}
Pyrite	Fe	0	0	0	0	0	0	0
	S	0.607(201)	0	0	0	0	0.536(126)	-0.003(88)
Marcasite	Fe	0	0	0	0	0	0	0
	S	0	-0.231(54)	0.168(51)	0	0	0.151(53)	0.064(45)

Table S2.VI. Hexadecapole population parameters for pyrite and marcasite.

	Atom	H_{40}	H_{41+}	H_{41-}	H_{42+}	H_{42-}	H_{43+}	H_{43-}	H_{44+}	H_{44-}
Pyrite	Fe	0.19(1)	0	0	0	0	-0.320(9)	-0.03(1)	0	0
	S	-0.01(7)	0	0	0	0	-0.18(7)	-0.01(5)	0	0
Marcasite	Fe	0.20(2)	0	0	0.46(2)	0.03(1)	0	0	-0.16(1)	0.06(1)
	S	0.02(3)	0	0	0.03(3)	0.04(4)	0	0	-0.00(4)	0.01(3)

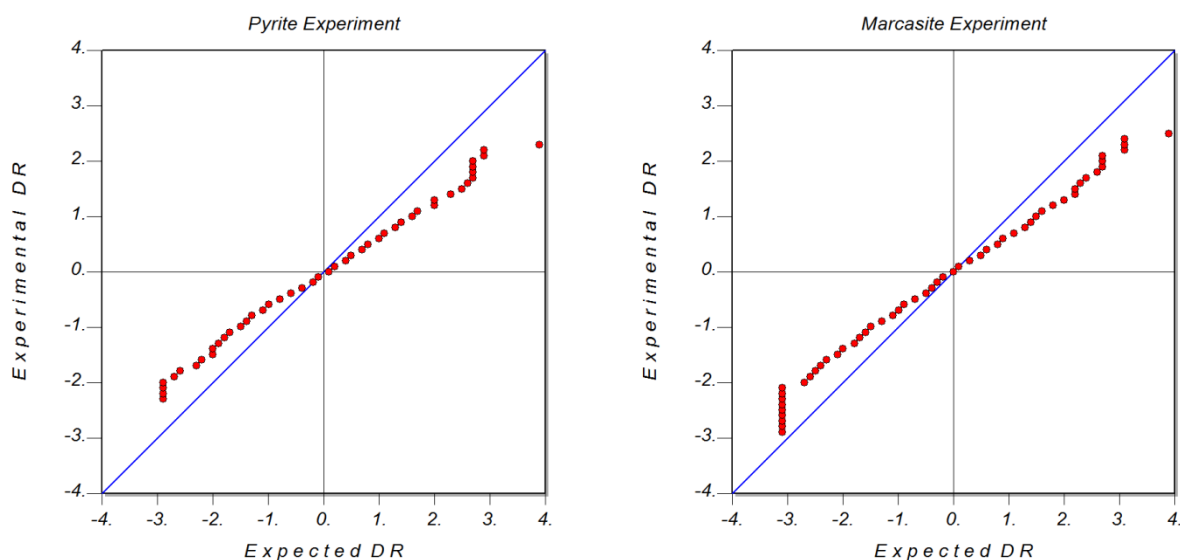


Figure S3: Normal probability plots from multipole refinement against the pyrite (left) and marcasite (right) data.

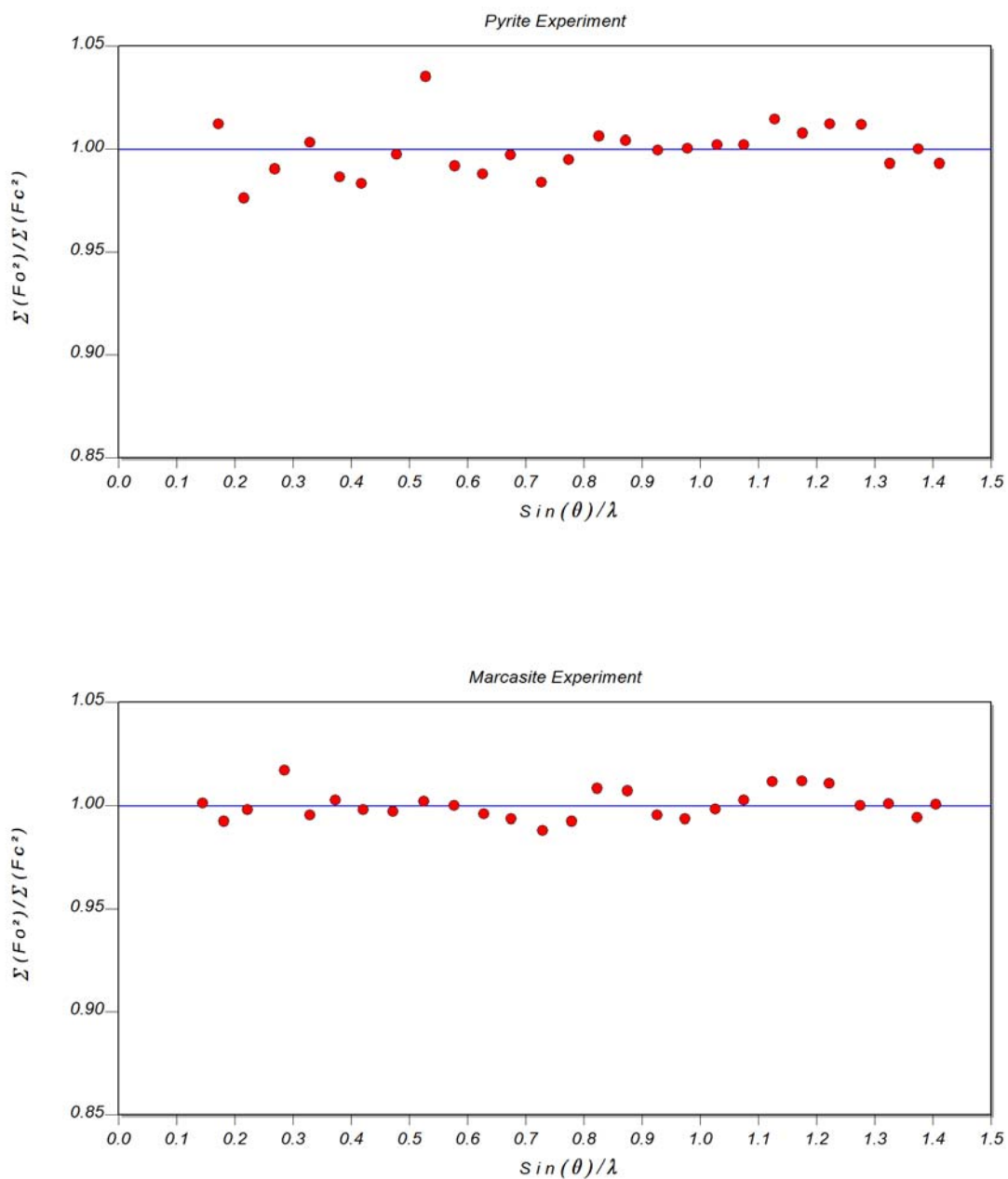


Figure S4: Scale factor variation (F_o^2/F_c^2) with resolution for data averaged within 0.05 \AA^{-1} intervals resulting from multipole refinement against the pyrite (top) and marcasite (bottom) data.

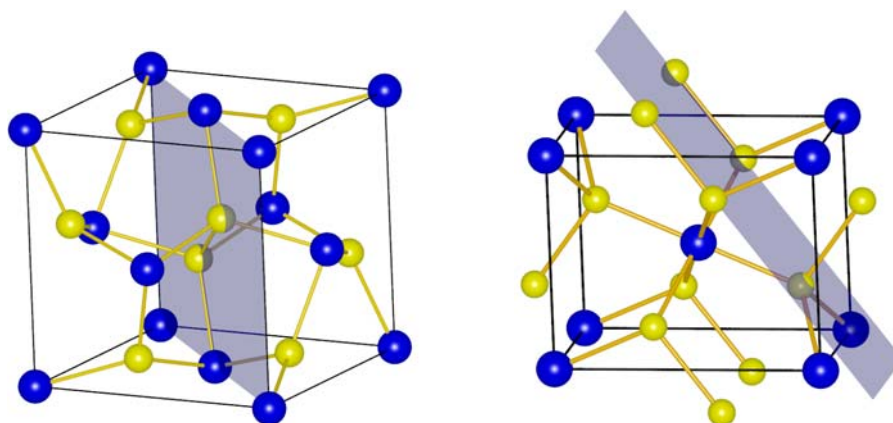


Figure S5: Planes containing the S-S interactions in FeS₂ pyrite (left) and marcasite (right) used for plotting.

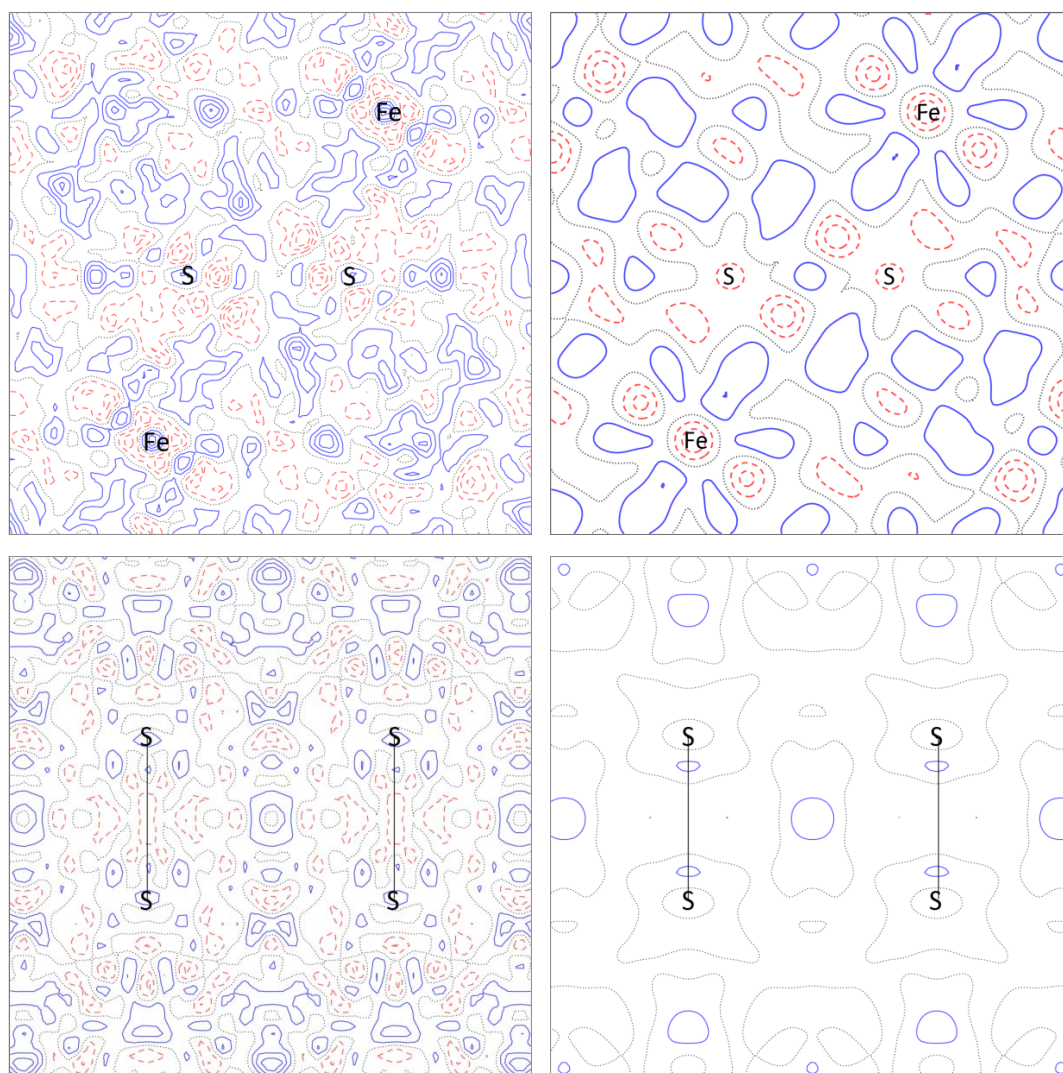


Figure S6: Experimental residual density for all data (left) and for reflections up to 0.8 Å⁻¹ (right) in a plane containing the S-S dimer (Figure S5) for pyrite (top) and marcasite (bottom). The increment in the contours is 0.1 eÅ⁻³. Positive

contours are plotted with full, blue lines. Negative contours are plotted with dashed, red lines. The dotted, black lines are the zero contours.

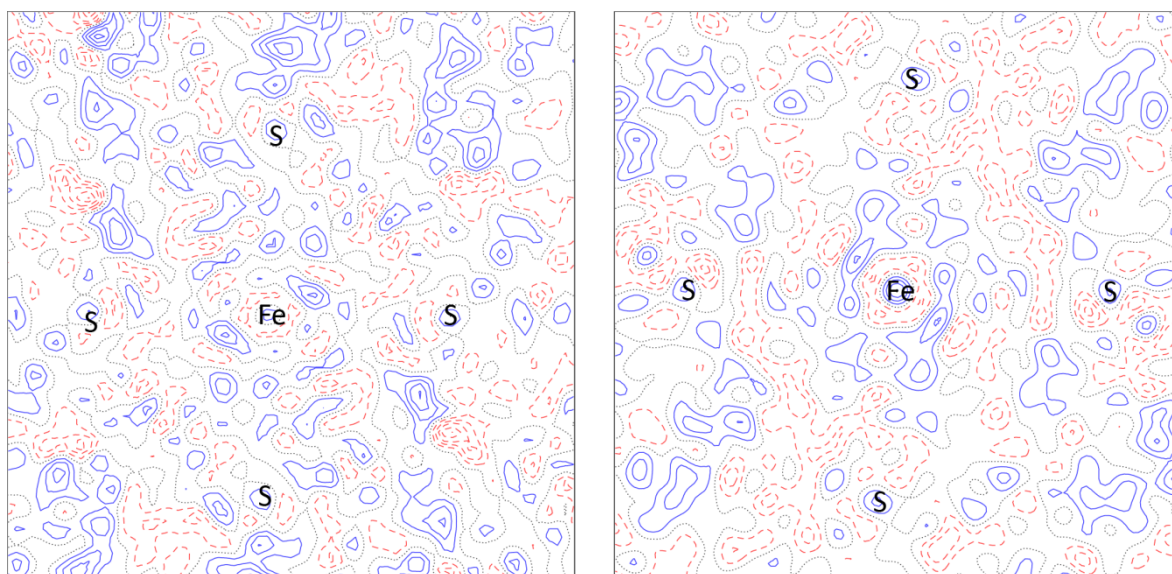


Figure S7: Residual density for all data in the FeS₄ plane of pyrite (left) and marcasite (right) obtained from multipole refinement against experimental data. The increment in the contours is 0.1 eÅ⁻³. Positive contours are plotted with full, blue lines. Negative contours are plotted with dashed, red lines. The dotted, black lines are the zero contours.

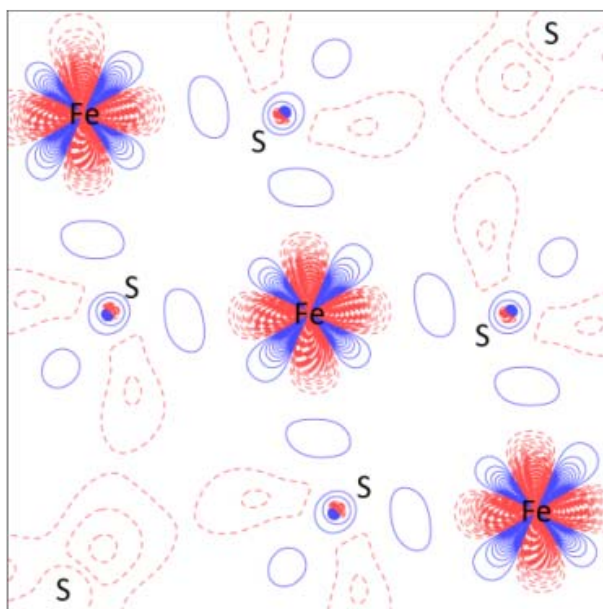


Figure S8: Static deformation densities for the equatorial Fe-S interactions in marcasite obtained from multipole refinement against the experimental data. The increment in the contours is 0.1 eÅ⁻³. Positive contours are plotted with full, blue lines. Negative contours are plotted with dashed, red lines.

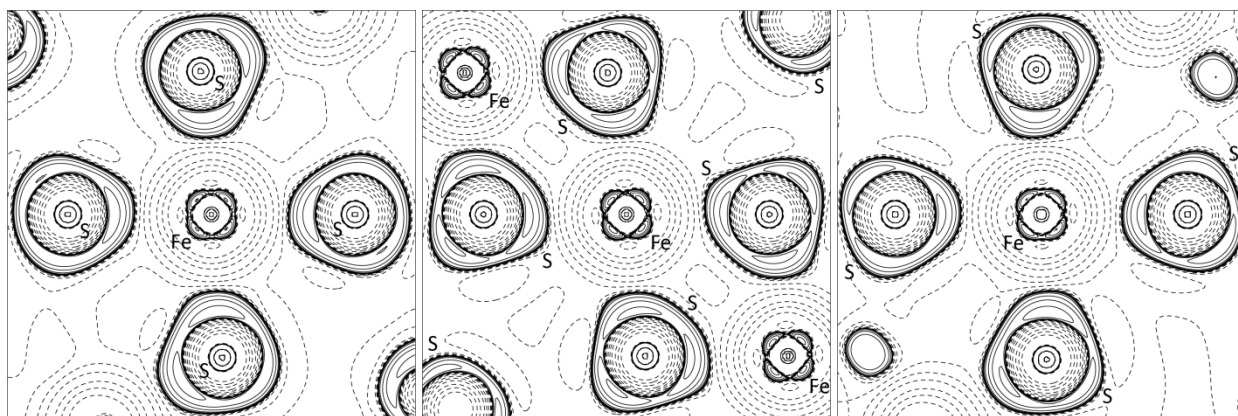


Figure S9: Experimental contour plots of $-\nabla^2\rho$ for the FeS_4 -plane in pyrite (left), the FeS_4 -plane containing the four equatorial Fe-S interactions (middle) and the two equatorial and two axial Fe-S interactions (right) in marcasite. The contour level is 2×10^7 ($x = 0,1,2,4$ and $y = -3,-2,-1,0,1,2$). Dashed contour lines represent positive values and solid lines represent negative values.

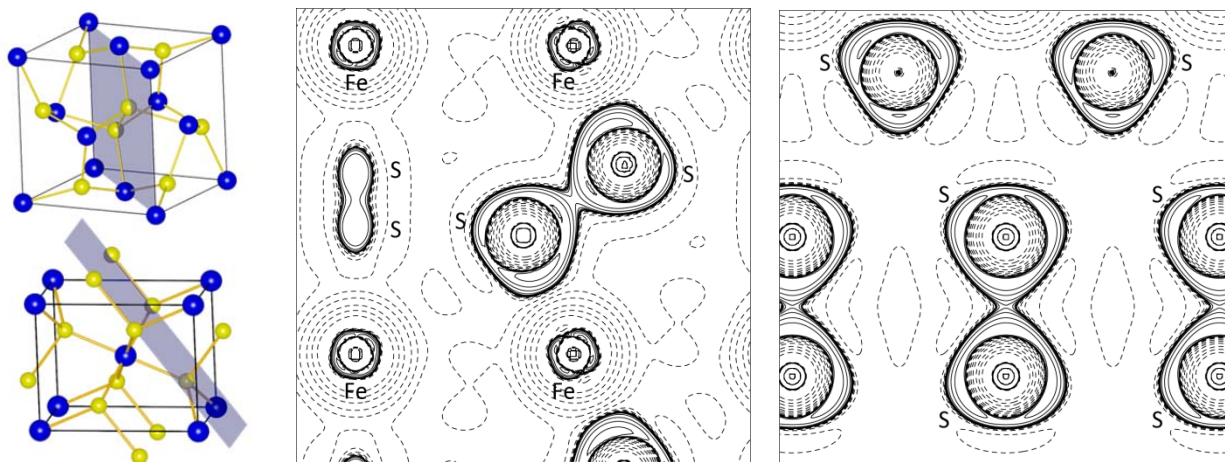


Figure S10: Contour plots of the Laplacian in a plane containing the S-S dimer in pyrite (left) and marcasite (right). In pyrite the plane is defined by the two S atoms along the body diagonal and the two bonded Fe atoms on opposing face centers (top). In marcasite the plane is defined by two pairs of neighboring S-S dumbbells as shown (bottom). The contour level is 2×10^7 ($x = 0,1,2,4$ and $y = -3,-2,-1,0,1,2$). Dashed contour lines represent positive values and solid lines represent negative values.

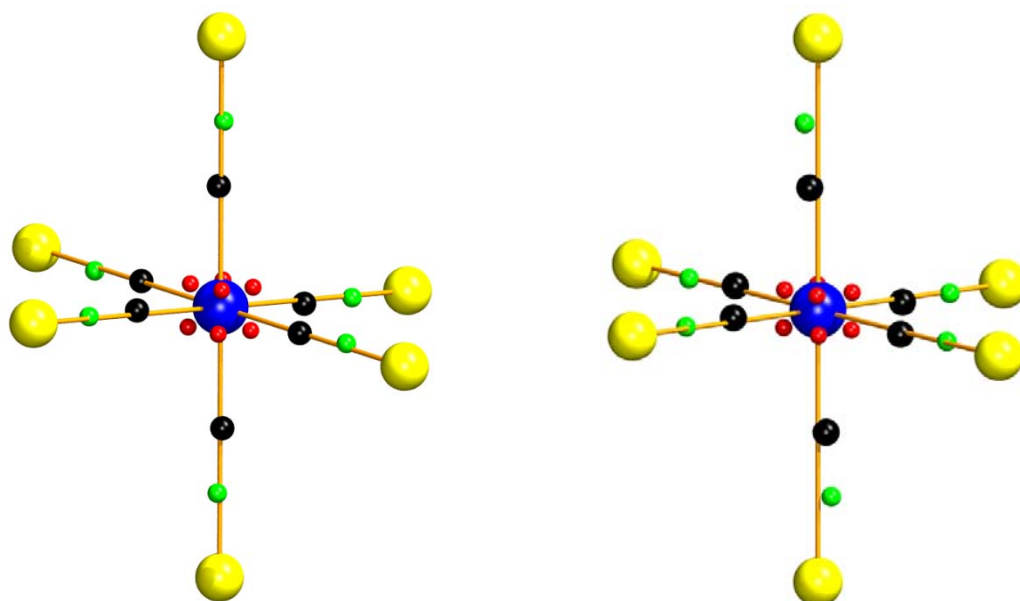


Figure S11: Topology of $\nabla^2\rho$ for the Fe atom and the Fe-S interactions of pyrite (left) and marcasite (right) resulting from multipole refinement against experimental data. Blue and yellow spheres represent Fe and S atoms, respectively. The small black spheres mark the positions of the bcps while red and green spheres mark the positions of the charge accumulation sites found within the Fe and S VSCC, respectively. For marcasite, the two vertical Fe-S interactions correspond to the shorter (axial) Fe-S bonds and the two horizontal (equatorial) sulfur atoms pointing towards the viewer form the smaller S-Fe-S opening angle ($\alpha \sim 82^\circ$).

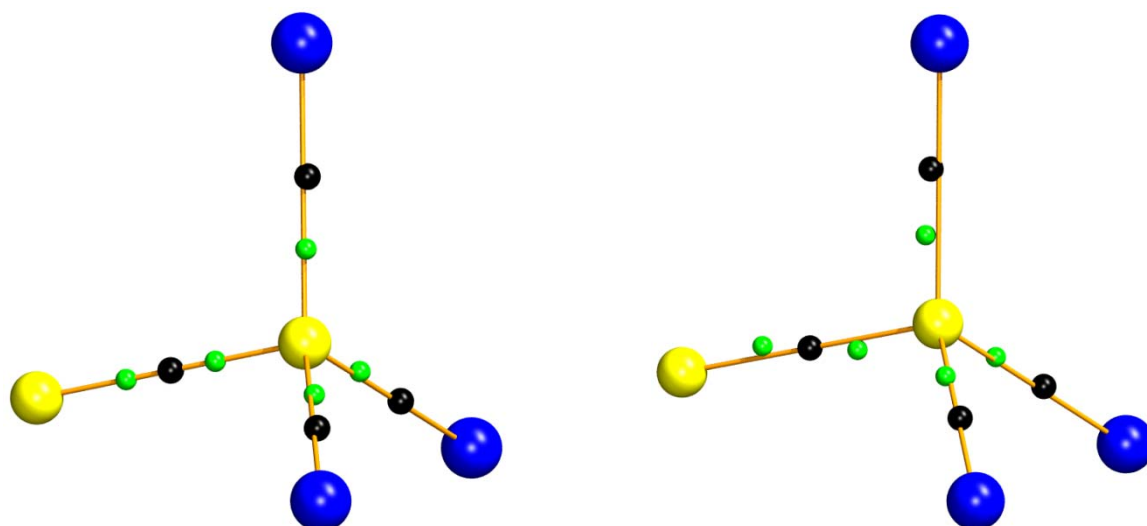


Figure S12: Topology of $\nabla^2\rho$ for the S atom in pyrite (left) and marcasite (right) resulting from multipole refinement against experimental data. Blue and yellow spheres represent Fe and S atoms, respectively. The small black spheres mark the positions of the bcps while the green spheres mark the positions of the minima in $\nabla^2\rho$, i.e. of charge accumulation found within the S VSCC. For marcasite, the vertical Fe-S interaction pointing upwards corresponds the shorter (axial) Fe-S bond.

II. Multipole refinement against theoretical data

Table S3: Results from multipole refinement against theoretical structure factors obtained from periodic, *ab-initio* DFT calculations in *WIEN2K* for the pyrite and marcasite structure. The data have been refined against two different multipole models: Model 1 is based on the assumption that the two 4s electrons on Fe have been fully transferred to S and only the 3d shell on Fe is used for the description of the valence electrons in iron. The description of S is based on the standard radial functions. Model 2 corresponds to the model used for the multipole refinement in the main paper and assumes neutral atoms as a starting point, but allowing for charge transfer between the sulfur valence and the 3d and 4s valence shell on Fe, which are treated separately. Modified radial functions are used for the description of S. All refinements are based on F and $\sin\theta/\lambda(=s) < 1.75 \text{ \AA}^{-1}$.

	Pyrite		Marcasite	
	Model 1	Model 2	Model 1	Model 2
$R(F), R(F^2)$	0.19 %, 0.26 %	0.09 %, 0.11 %	0.19 %, 0.30 %	0.08 %, 0.11 %
$\pm\Delta\rho (e/\text{\AA}^3)_{s < 1.75}$	-0.636 / +0.499	-0.315 / +0.178	-0.647 / +0.316	-0.270 / 0.135
$\pm\Delta\rho (e/\text{\AA}^3)_{s < 0.8}$	-0.327 / +0.090	-0.073 / +0.070	-0.325 / +0.092	-0.087 / +0.068
$\kappa(\text{Fe}, 3d)$	0.992(1)	0.9924(4)	0.994(1)	0.9947(3)
$\kappa'(\text{Fe}, 3d)$	1.047(6)	1.024(3)	1.046(5)	1.028(2)
$\kappa(\text{S})$	0.959(1)	0.9854(4)	0.958(1)	0.9874(4)
$\kappa'(\text{S})$	0.736(8)	0.967(3)	0.749(6)	0.954(3)
$P_{\text{val}}(\text{Fe}), P_{\text{val}}(4s)$	6.10(2), 0	6.009(6), 1.74(2)	6.10(1), 0	5.978(5), 1.84(2)
$P_{\text{val}}(\text{S})$	6.950(8)	6.123(8)	6.951(6)	6.090(7)
$Q_{\text{MM}}(\text{Fe})$	+1.90(2)	+0.25(2)	+1.90(1)	+0.18(2)
$Q_{\text{MM}}(\text{S})$	-0.950(8)	-0.123(8)	-0.951(6)	-0.090(7)
$Q_{\text{ATB}}(\text{Fe})$	+0.96	+0.59	+0.97	+0.56
$Q_{\text{ATB}}(\text{S})$	-0.48	-0.29	-0.48	-0.27
$\rho, \nabla^2\rho(\text{Fe-S1})$	0.531, 4.298	0.536, 5.593	0.611, 5.149	0.558, 5.709
$AIL_{\text{Fe-bcp}}, AIL_{\text{S-bcp}}$	1.039, 1.224	1.017, 1.246	1.021, 1.215	1.015, 1.220
$\rho, \nabla^2\rho(\text{Fe-S2})$	-	-	0.587, 4.973	0.548, 5.483
$AIL_{\text{Fe-bcp}}, AIL_{\text{S-bcp}}$	-	-	1.025, 1.228	1.016, 1.237
$\rho, \nabla^2\rho(\text{S-S})$	0.756, 0.365	0.850, -1.046	0.720, 1.461	0.774, -0.361
$AIL_{\text{Sb-bcp}}$	1.080	1.080	1.106	1.106

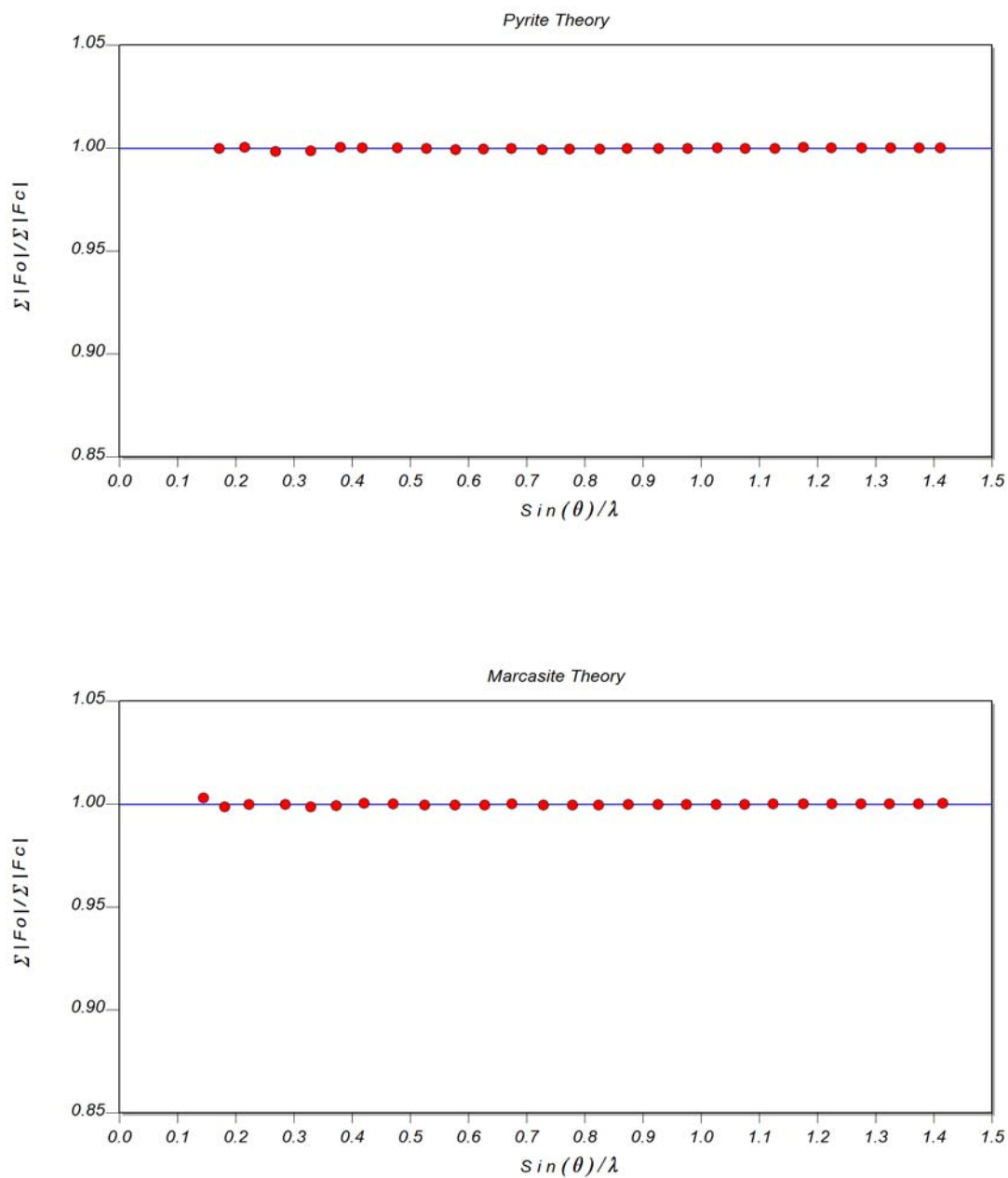


Figure S13: Scale factor variation (F_o/F_c ; refinement against F) with resolution for theoretical data averaged within 0.05 \AA^{-1} intervals resulting from multipole refinement against the pyrite (top) and marcasite (bottom) data.

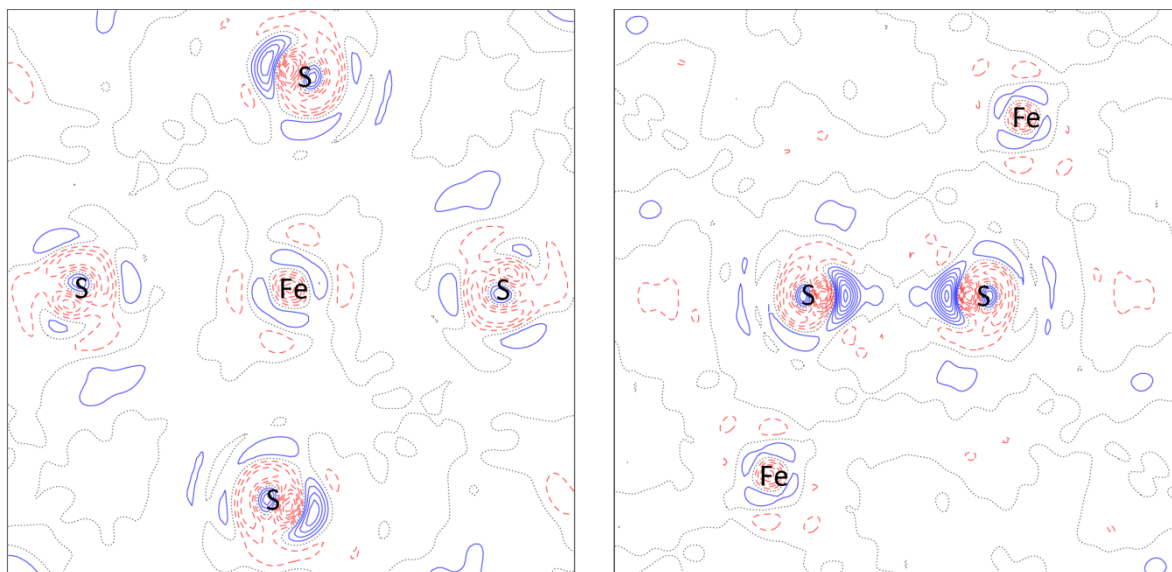


Figure S14: Residual density for all data in the FeS_4 plane (left) and a plane containing the S-S dimer (right) in pyrite obtained from multipole refinement against theoretical data. The increment in the contours is $0.02 \text{ e}\text{\AA}^{-3}$. Positive contours are plotted with full, blue lines. Negative contours are plotted with dashed, red lines. The dotted, black lines are the zero contours.

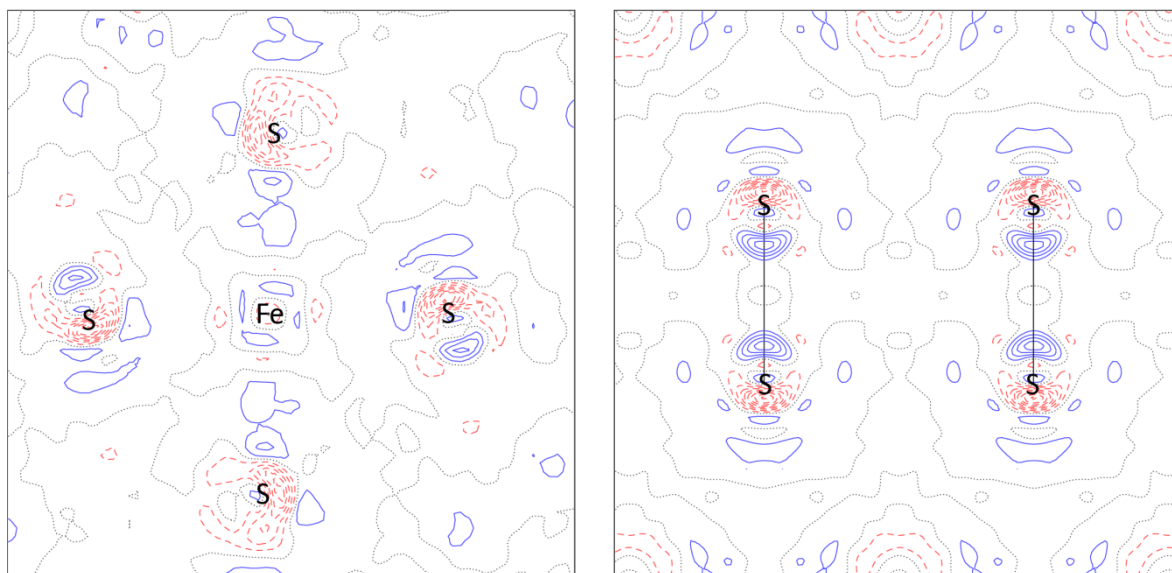


Figure S15: Residual density for all data in the FeS_4 plane (left) and a plane containing the S-S dimer (right) in marcasite obtained from multipole refinement against theoretical data. The increment in the contours is $0.02 \text{ e}\text{\AA}^{-3}$. Positive contours are plotted with full, blue lines. Negative contours are plotted with dashed, red lines. The dotted, black lines are the zero contours.

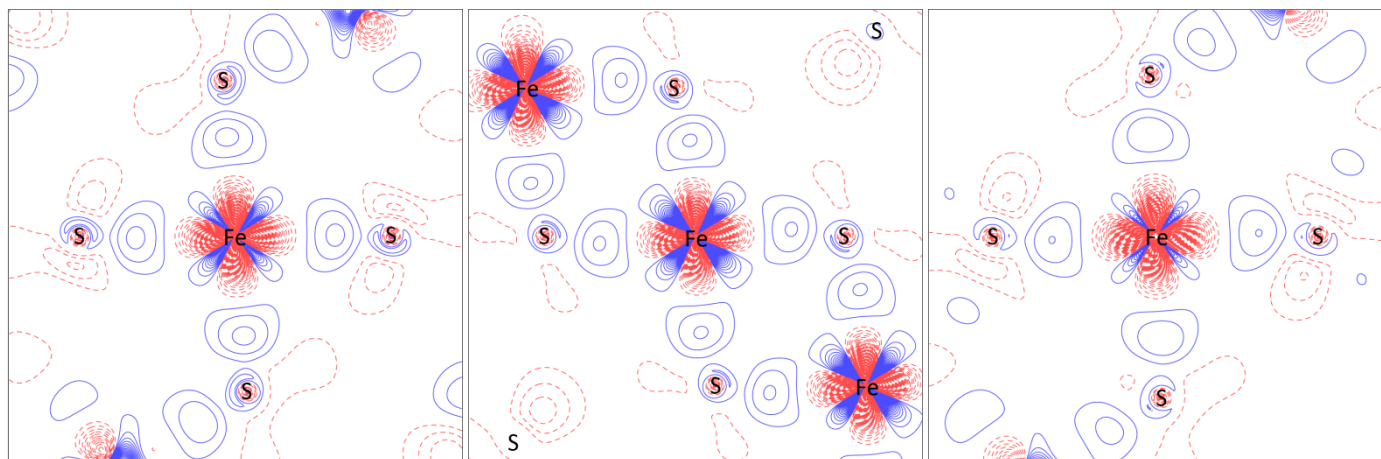


Figure S16: Static deformation densities for the Fe-S interactions in pyrite (left), the equatorial (middle), and axial and equatorial (right) Fe-S interactions in marcasite obtained from multipole refinement against theoretical data. The increment in the contours is $0.05 \text{ e}\text{\AA}^{-3}$. Positive contours are plotted with full, blue lines. Negative contours are plotted with dashed, red lines.

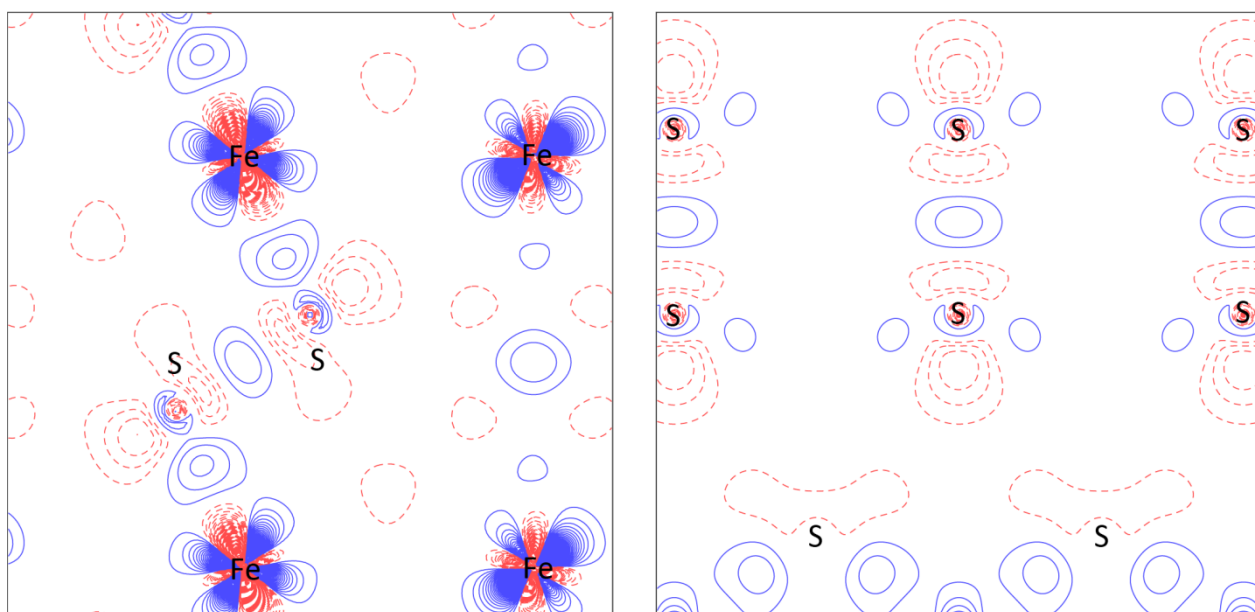


Figure S17: Static deformation density for the S-S interaction in pyrite (left) and marcasite (right) obtained from multipole refinement against theoretical data. The contour increment is $0.05 \text{ e}\text{\AA}^{-3}$. Positive contours are plotted with full, blue lines, negative contours with dashed, red lines.

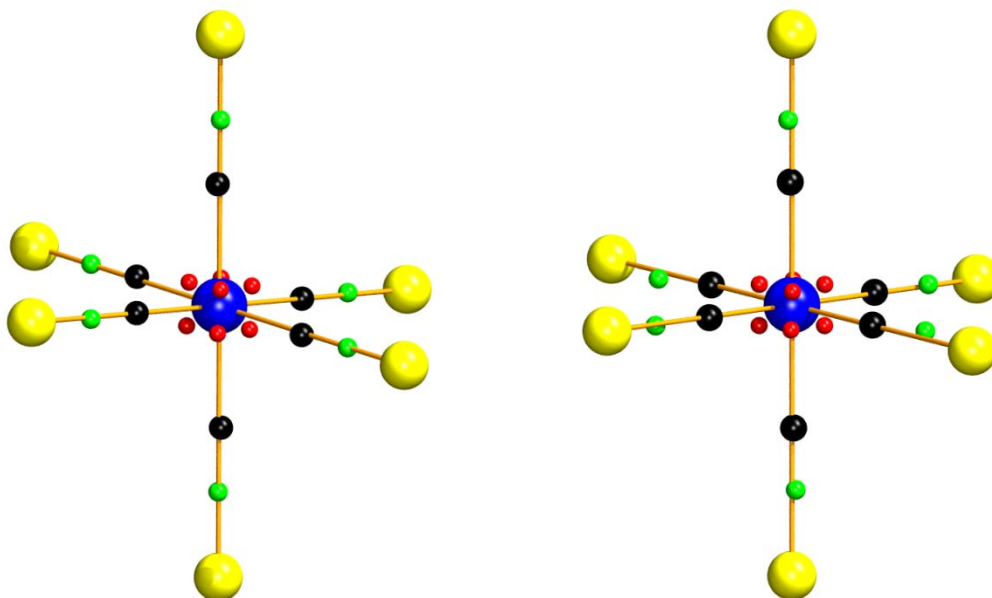


Figure S18: Topology of $\nabla^2\rho$ for the Fe atom and the Fe-S interactions of pyrite (left) and marcasite (right) resulting from multipole refinement against theoretical data. Blue and yellow spheres represent Fe and S atoms, respectively. The small black spheres mark the positions of the bcps while red and green spheres mark the positions of the minima in $\nabla^2\rho$, i.e. of charge accumulation sites found within the Fe and S VSCC, respectively. For marcasite, the two vertical Fe-S interactions correspond to the shorter (axial) Fe-S bonds and the two horizontal (equatorial) sulfur atoms pointing towards the viewer form the smaller S-Fe-S opening angle ($\alpha \sim 82^\circ$).

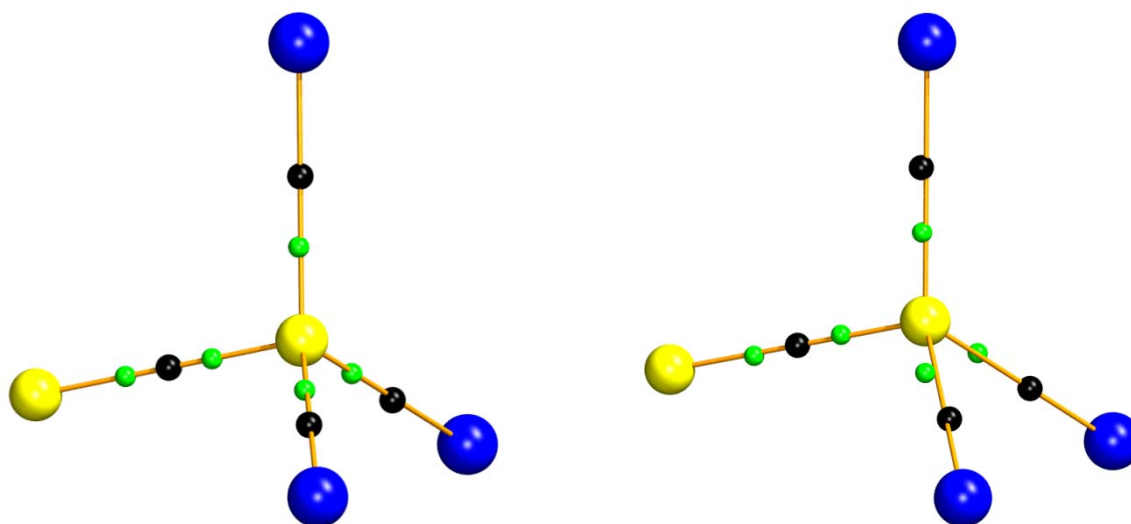


Figure S19: Topology of $\nabla^2\rho$ for the S atom in pyrite (left) and marcasite (right) resulting from multipole refinement against theoretical data. Blue and yellow spheres represent Fe and S atoms, respectively. The small black spheres mark the positions of the bcps while the green spheres mark the positions of the minima in $\nabla^2\rho$, i.e. of charge accumulation found within the S VSCC.

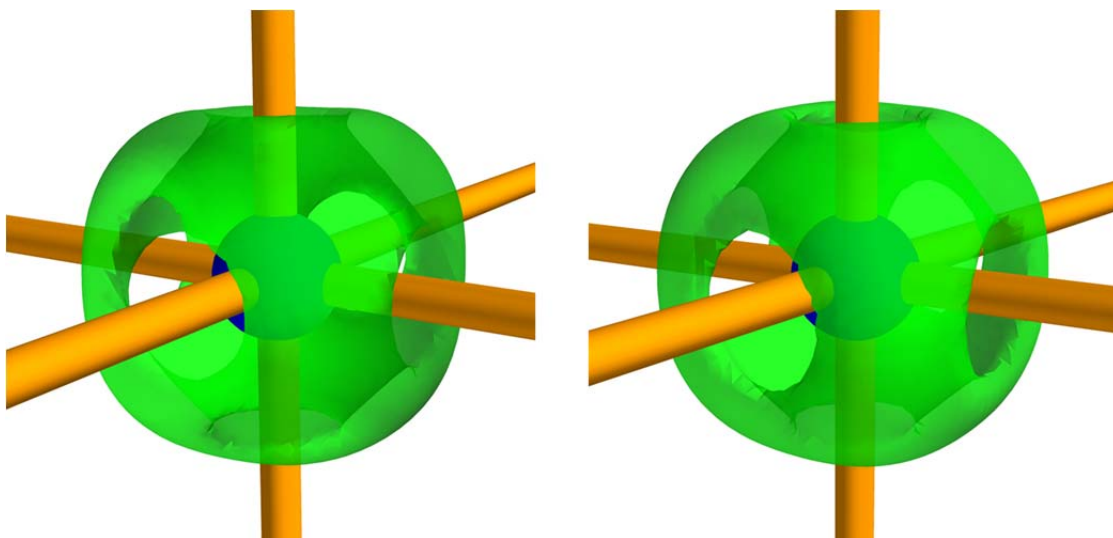


Figure S20: Three-dimensional plot of the theoretical Laplacian for Fe in pyrite (left) and marcasite (right) at isocontour values of $-500 \text{ e}/\text{\AA}^5$.

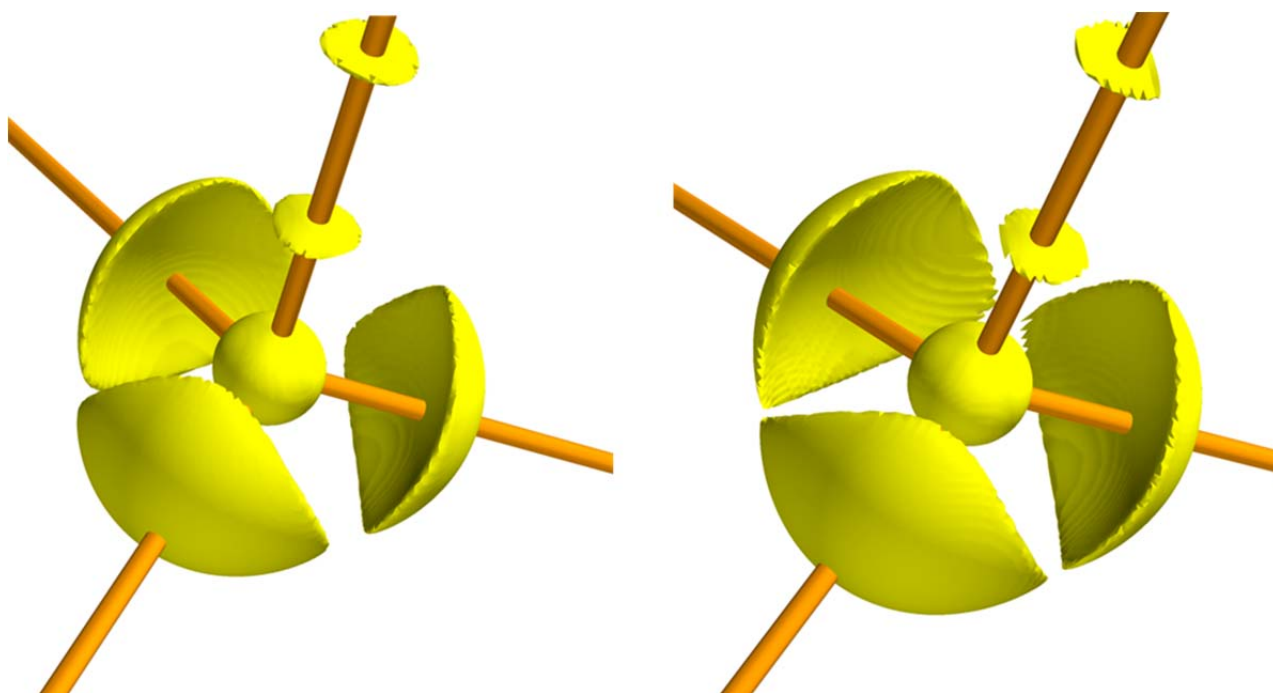


Figure S21: Three-dimensional plot of the theoretical Laplacian for the S-atom in pyrite (left) and marcasite (right) at isocontour values of $-6.4 \text{ e}/\text{\AA}^5$ (left) and $-6.2 \text{ e}/\text{\AA}^5$ (right). The S-S bond points towards the top right corner.

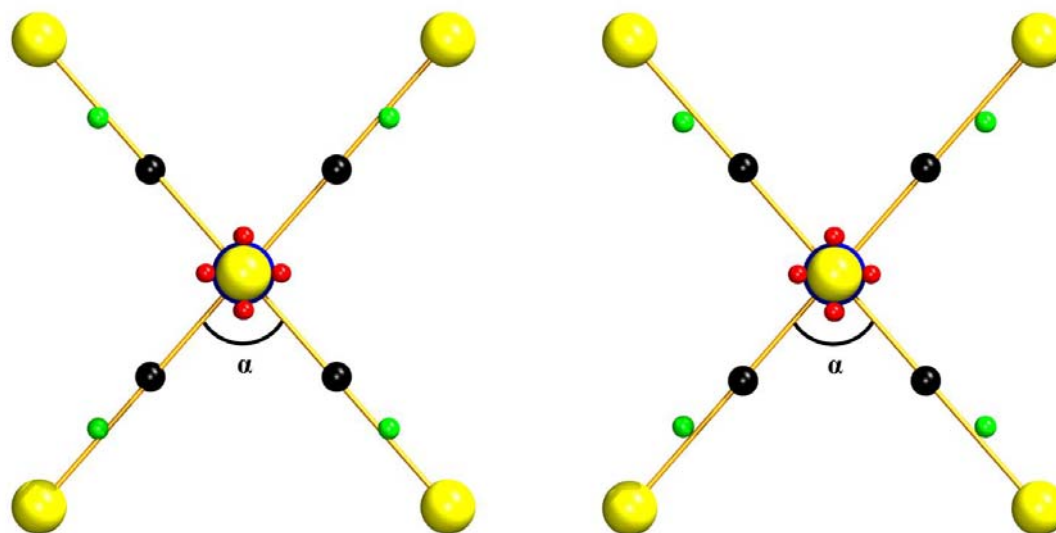


Figure S22: Topology of $\nabla^2\rho$ for the equatorial (long) Fe-S interactions in marcasite resulting from multipole refinement against experimental (left) and theoretical (right) data. Blue and yellow spheres represent Fe and S atoms, respectively. The small black spheres mark the positions of the bcps, the red spheres are the Fe VSCC maxima and the green spheres mark the positions of the S VSCC maxima. The smaller S-Fe-S opening angle, $\alpha \sim 82^\circ$, is marked.

Table S4: Maxima in the VSCC of Fe (upper rows) and S (lower rows) in marcasite (*m*) and pyrite (*p*) evaluated for the electron density resulting from multipole refinement against experimental (experiment) and theoretical (theory) data. The value of the density, ρ_{\max} , and the negative Laplacian, $-\nabla^2\rho_{\max}$, together with the distance to the atomic center, d , is reported for each maximum. Also the number of occurrences per atom of each type of maximum is given.

		occurrence	ρ_{\max} ($\text{e}\text{\AA}^{-3}$)		$-\nabla^2\rho_{\max}$ ($\text{e}\text{\AA}^{-5}$)		d (\AA)	
			experiment	theory	experiment	theory	experiment	theory
Fe	<i>m</i>	2	27.16	25.62	1395.4	1137.7	0.312	0.316
	<i>m</i>	2	25.69	26.17	1180.9	1213.4	0.316	0.315
	<i>m</i>	4	26.16	25.87	1277.8	1160.45	0.314	0.316
	<i>p</i>	2	26.04	26.11	1203.3	1180.1	0.315	0.315
	<i>p</i>	6	25.99	25.68	1217.4	1149.1	0.315	0.316
S(-S)	<i>m</i>	1	1.187	1.102	7.50	6.46	0.720	0.726
	<i>p</i>	1	1.260	1.124	8.52	6.74	0.720	0.729
S(-Fe1)	<i>m</i>	1	1.325	1.251	12.2	10.2	0.709	0.709
S(-Fe2)	<i>m</i>	2	1.236	1.256	9.96	10.4	0.711	0.710
	<i>p</i>	3	1.256	1.268	11.8	10.9	0.713	0.709

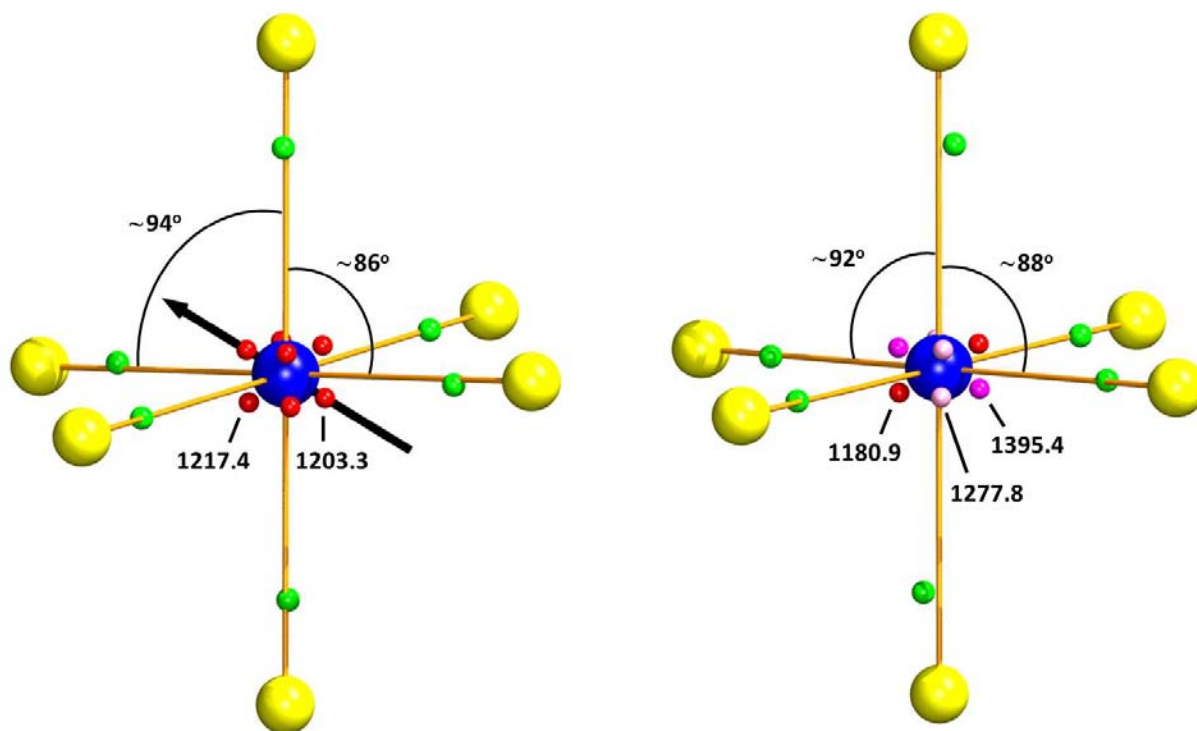


Figure S23: Experimental topology of $-\nabla^2\rho$ Fe in pyrite (left) and marcasite (right). Blue and yellow spheres represent Fe and S, respectively. The red and pink spheres mark the positions of the Fe VSCC maxima and the green spheres correspond to the positions of the S VSCC maxima. The black arrow shows the direction of the 3-fold rotation axis.

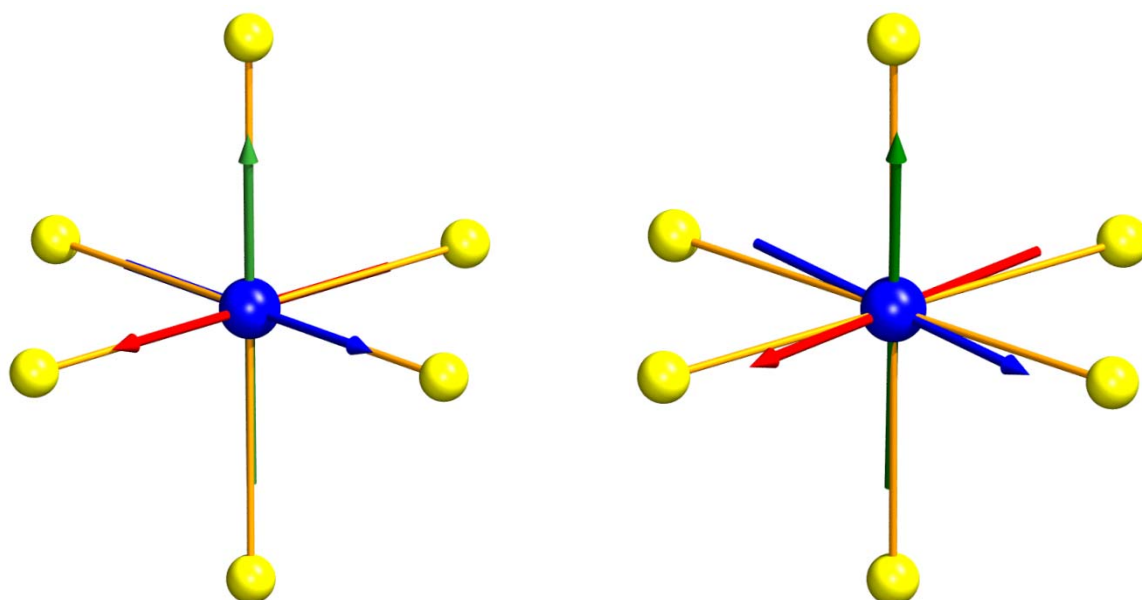


Figure S24: Local coordinate system for *d*-orbital evaluation of pyrite (left) and marcasite (right) resulting from multipole refinement against theoretical data. *x*, *y*, *z* axes are represented by red, blue and green arrows, respectively. For marcasite, the short Fe-S interaction is pointing vertically along the *z* axis.

Table S5: d-orbital populations obtained directly from DFT calculations in WIEN2K based on the experimental geometry and on a local coordinate system centered on Fe for which the z axis points exactly along the short Fe-S bond in marcasite and along one of the Fe-S bonds in pyrite. The x and y axes are placed so that they are as close as possible and equidistant from two of the equatorial Fe-S bonds in marcasite and from two of the remaining Fe-S bonds in pyrite.

	Pyrite		Marcasite	
	Population (e)	% population	population	% population
d_{xy}	1.525	24.54 %	1.638	26.38 %
d_{xz}	1.516	24.39 %	1.461	23.53 %
d_{yz}	1.515	24.38 %	1.461	23.53 %
d_{z^2}	0.828	13.33 %	0.878	14.15 %
$d_{x^2-y^2}$	0.830	13.36 %	0.771	12.41 %
P_{total}	6.215	100 %	6.208	100 %

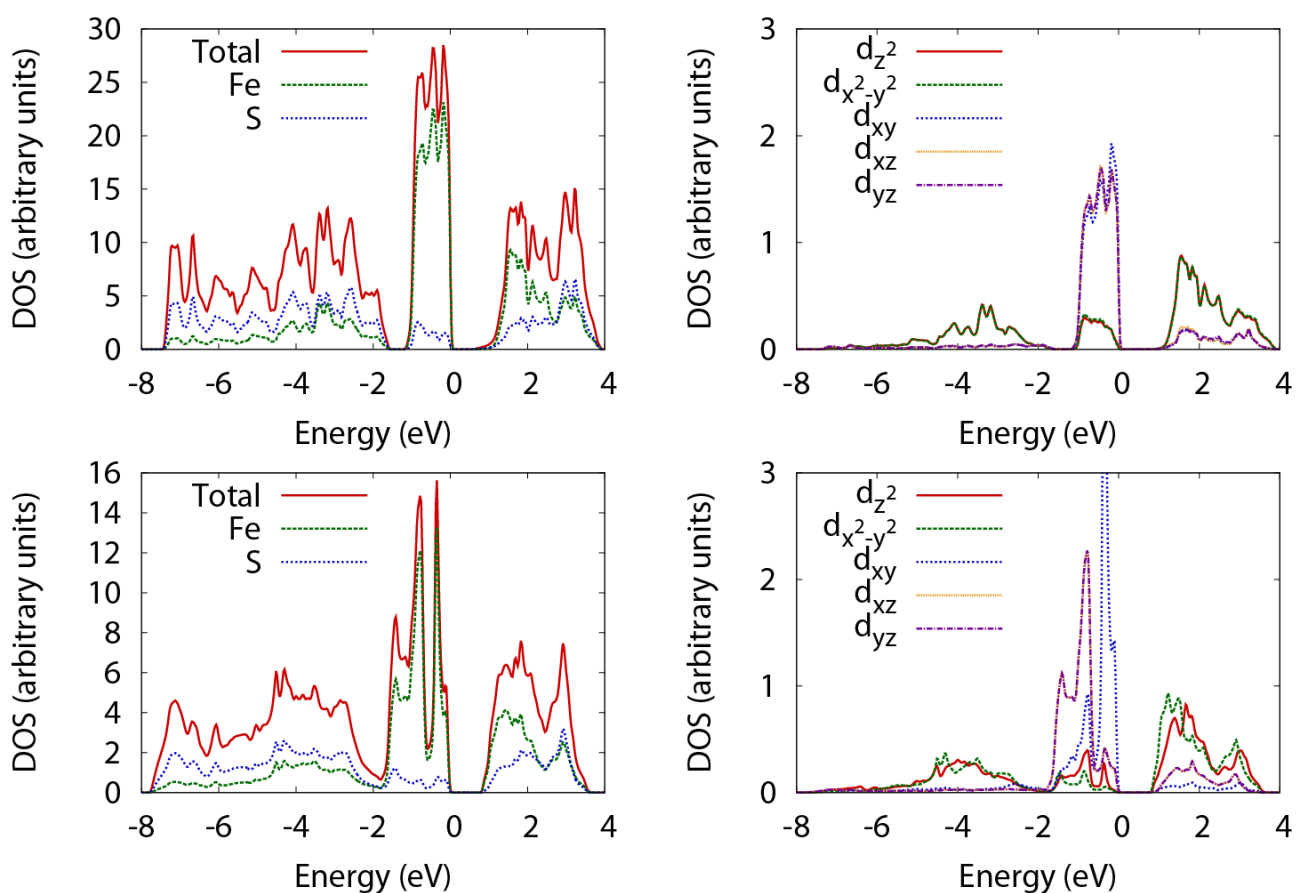


Figure S25: Total and atom-projected DOS (left) and Individual Atomic Orbitals projected DOS of the Fe d orbital states (right) for pyrite (top) and marcasite (bottom). The results have been obtained from DFT calculations in WIEN2k using the experimental FeS_2 geometries and employing the local coordinate systems described in the caption for Table S5.